Exploring Source Structure with the Bordeaux VLBI Image Database Comparing Jet Directions with Optical-Radio Offset Vectors

Arnaud Collioud, P. Charlot, Sébastien Lambert

Exploring Source Structure with the Bordeaux VLBI Image Database

Comparing Jet Directions with Optical-Radio Offset Vectors

Arnaud Collioud[1], Patrick Charlot[1], Sébastien Lambert[2]

Abstract The Bordeaux VLBI Image Database provides to the international VLBI community almost 8,000 VLBI images of radio sources at S and X band and some others at K and Q band. Such images are of interest for astrometric and astrophysical applications, such as the determination of the VLBI jet direction. We developed a fully automatic method to extract this direction from any VLBI image, which we then applied to all BVID images, resulting in the production of 9,215 jet directions for 1,221 sources. Comparing the mean jet directions over all epochs at X band to the Gaia EDR3 (optical) − ICRF3 S/X (radio) offset vector directions indicates that the offset vector is aligned within 30° of the jet direction in roughly half of the sources, thereby confirming previous studies.

Keywords VLBI, Database, Imaging, Source Structure, Jet Direction, ICRF, Gaia

1 Introduction

Since 2008, the Bordeaux VLBI Image Database (BVID)[1] has made VLBI images of radio reference frame sources available to the international VLBI community [1, 2]. The vast majority of these images have been produced from RDV (Research & Development VLBA) or VLBA experiments. The BVID currently contains around 7,900 such images at S and X band (2.3 and 8.6 GHz), along with some at K and Q band (22 and 43 GHz), and associated data about source structure (compactness and structure index information), which are of interest for astrometric and astrophysical applications. Those images cover a period of time of more than 20 years and are available for a total of about 1,500 different sources.

Most of the sources show non-point-like structures on VLBI scales and often exhibit jets. The directions of these jets may be of interest for astrophysical studies, but also for astrometric scheduling purposes where one tries to mitigate the effect of source structure by avoiding observations with projected VLBI baselines aligned onto the jet directions. Section 2 presents a new method that we developed to automatically determine the jet direction from a VLBI map. In Section 3, we discuss the results derived when applying this method to the BVID images and the potential applications of such results. One of these is the study of the relation between the jet directions and the directions of the offset vectors revealed by comparing the Gaia Early Data Release 3 (EDR3) and S/X-band ICRF3 positions. This application is further investigated in Section 4.

2 Method to Determine Jet Direction

We developed a fully automatic pipeline to determine the jet direction from any VLBI map. The algorithm can be decomposed into several successive steps which are described below and also illustrated by Figure 1 (upper- and lower-left panels):

1. Read the source model (i.e., the CLEAN components) and some additional information from the image (map and beam size, residual map RMS

1. Laboratoire d'Astrophysique de Bordeaux, Université de Bordeaux, CNRS, France
2. SYRTE, Observatoire de Paris, Université PSL, Sorbonne Université, CNRS, France

[1] Available at https://bvid.astrophy.u-bordeaux.fr

noise). Our method does not require model-fitting of the source, a task which can be time-consuming and user-dependent when manually done.
2. Split the image plane into 10-degree azimuthal bins and sum the flux of the individual components in each bin to obtain the distribution of the flux with respect to the direction.
3. Compute the mean and the standard deviation of this flux distribution.
4. Repeat step 3 when considering the model components located outside an increasing radius (starting from the center of the map). The procedure stops when a certain flux cut-off is reached.
5. Compute the global weighted mean direction and error from the mean directions determined at each radius. This global direction ranges from 0 to 180° (anti-clockwise) and from 0 to −180° (clockwise).

At the end of the procedure, we also plot the global direction (from step 5 above) overlaid on the VLBI map to visually check that it is consistent with the morphology of the source, in particular with any detected jet-like structure (see Figure 1, lower-right panel).

3 Application to BVID Images

We applied our pipeline to all the images available in the BVID database. Overall, we determined 9,215 jet directions for 1,221 sources with the distribution between frequencies indicated in Table 1 below.

Table 1 Number of jet directions for each frequency band.

Band	S	X	K	Q	Total
Frequency (GHz)	2.3	8.6	22.0	43.0	
N sources	1,145	1,145	274	132	1,221
N jet directions	3,905	3,975	1,068	267	9,215

Almost all sources have jet directions available at two or more frequency bands. Thus, it is of interest to compare the jet directions in the different bands. For example, Figure 2 displays the jet directions determined for the source OJ287 (0851+202) at the four bands. In this case, the directions are consistent (within the errors) between bands even if the maps result from data at different epochs (2020 for S and X band and 2002 for K and Q band). We plan to develop further this comparison between bands in a study to come.

In addition, we can also take advantage of the long time span of the BVID data to produce time series of the jet direction for each source at each frequency band. Studying those may reveal time variability, and even periodicity, that could possibly be tied to the physical properties of the source jet and/or its inner black hole. An example of such time series, again for the source OJ287, is shown in Figure 3. Overall, the jet direction exhibits no strong variation with time, but a long-term trend is seen at S and X band between 2007 and 2017. A systematic study of the time series is out of the scope of this work but is planned for the near future.

Finally, we computed for all sources and all bands the mean direction over all epochs (i.e., the temporal mean). Those directions will be used in the next section for comparison with the optical-radio offset vector orientations.

4 Comparison between Jet Directions and Optical-Radio Offset Vectors

Gaia is a space mission of the European Space Agency, launched in 2013, dedicated in particular to measure the positions, distances, and motions of several billions of objects in the sky. Especially, more than 1.5 million extragalactic sources are available in the Gaia EDR3 delivered on 3 December 2020 [3]. After cross-matching the EDR3 catalog (optical) with the ICRF3 catalog at S/X-band (radio), we obtained a list of 3,477 common sources. For each source in that list, we computed the optical-to-radio offset vector angle, illustrated in Figure 4, in the same way as for the comparison of the ICRF3 to Gaia DR2 catalogs in [5]. The distribution of the offset vector angles (Figure 5, left panel) shows a roughly uniform distribution, but with an excess at 0° and 180°, i.e., along the declination axis, which is likely due to observing network effects.

From the results of Section 3, we also computed the distribution of the BVID jet directions at X band, which is displayed in Figure 5 (right panel). As before, the jet direction distribution exhibits peaks at 0° and 180°, most probably also caused by network effects.

With this information, we are now able to compare the BVID jet direction at X band and the optical-radio offset vector angle source by source (see Figure 4). The distribution of the difference between these an-

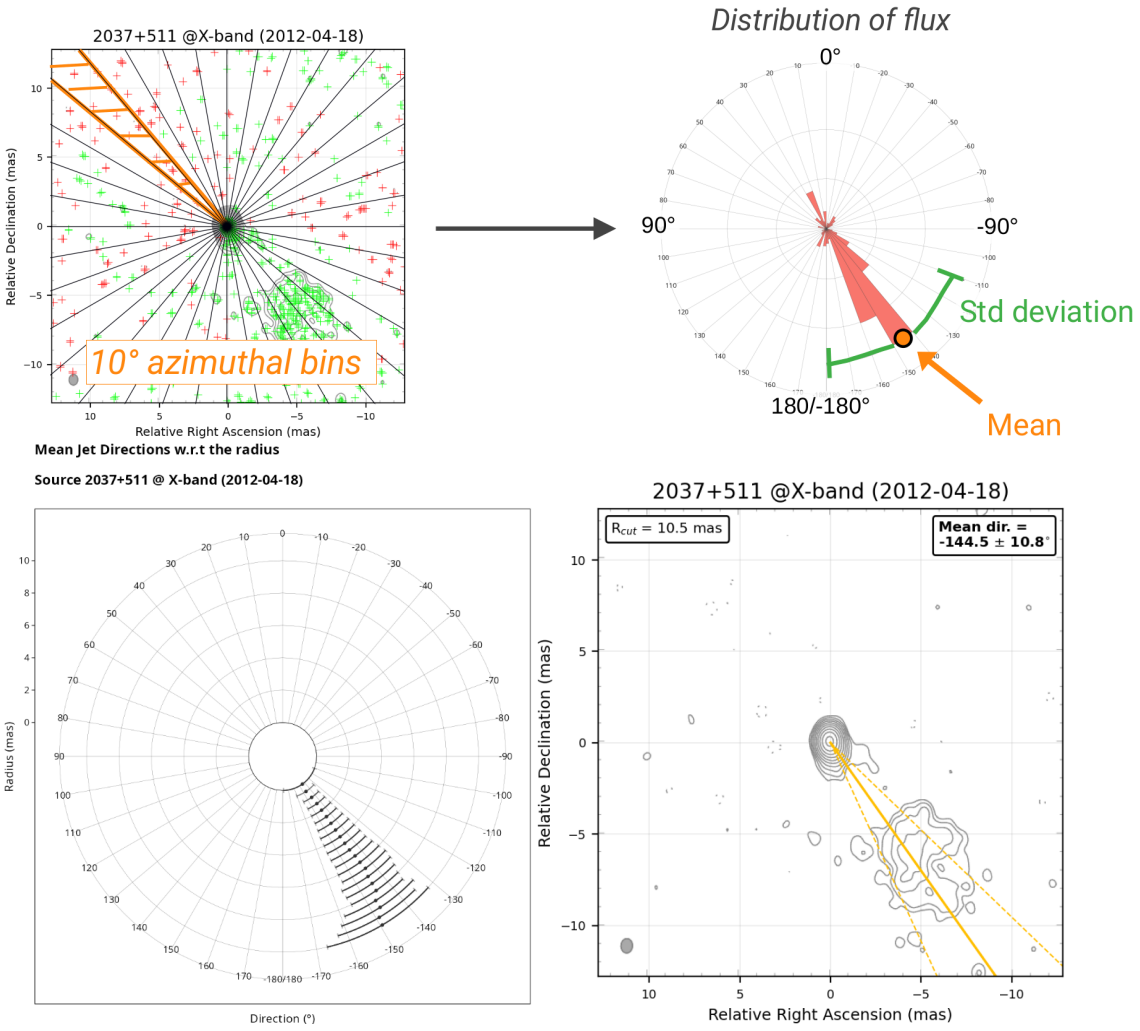

Fig. 1 Application of the jet-determination algorithm to the VLBI map of the source 2037+511 observed on 2012-04-18 at X band. (Top-left) View of the image plane sliced into 10-degree azimuthal bins. (Top-right) Azimuthal flux distribution after summing the flux of the components in each bin. The important values are the mean and standard deviation of this distribution. (Bottom-left) Plot of the individual mean directions and errors as a function of the increasing radius. (Bottom-right) Global mean direction ($-144.5 \pm 10.8°$) overlaid on the underlying jet-like structure.

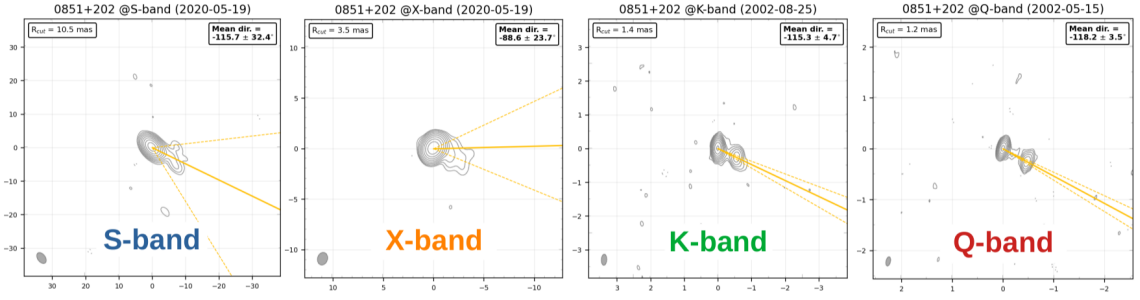

Fig. 2 Example of the jet directions computed from four images at S, X, K, and Q band of the source OJ287 (0851+202). The jet directions are found to be consistent within the error bars, although the maps are not from the same epoch.

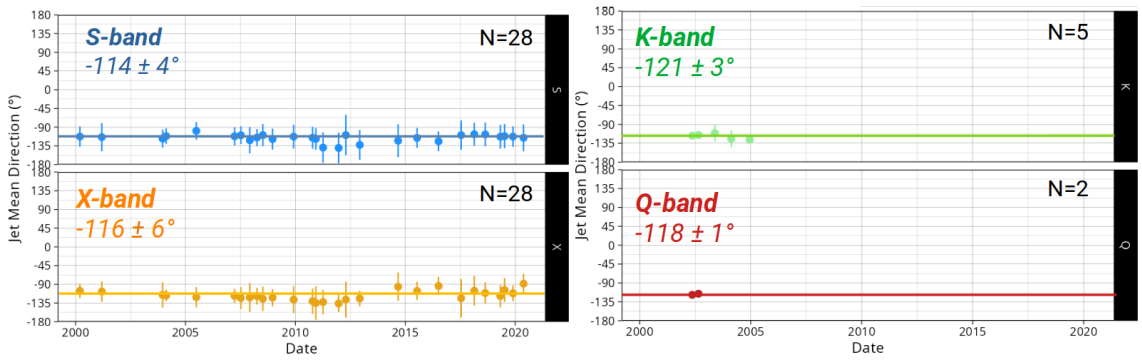

Fig. 3 Example of jet direction time series for the source OJ287 (0851+202) at S, X, K, and Q band. For each time series, the mean jet direction over all epochs and its error are computed. The mean jet directions are consistent at the four bands for this source.

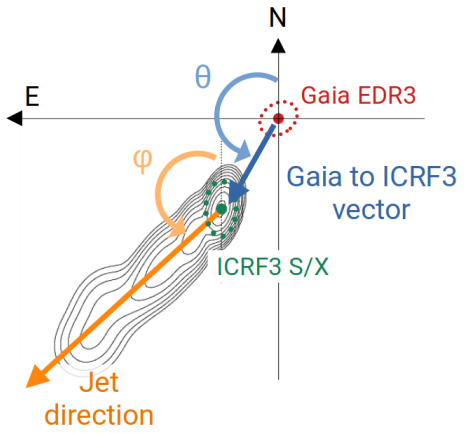

Fig. 4 Illustration of the comparison between the Gaia EDR3 and ICRF3 S/X-band positions, resulting in the optical-radio offset vector direction θ. This angle may be compared to the jet direction φ. It is assumed here that the ICRF3 position is located at the peak of the brightness distribution. The angle difference between θ and φ is small in this case, indicating that the jet and the optical-radio offset vector are almost aligned.

gles is plotted in Figure 6 (left panel) for the 865 common sources. From the plot shown, we deduce that the optical-radio offset vector predominantly aligns with the jet direction. This alignment is within a range of $\pm 30^\circ$ for almost half of the sample (393 sources), with 253 and 140 sources in the same and opposite direction, respectively.

This result confirms the conclusions from previous studies, which used other VLBI catalogs, other Gaia data releases, and/or other methods for computing the jet directions [4, 6, 7, 8, 9]. The specificity of the current work is that the VLBI positions and jet directions were obtained from data at the same frequency band.

To go further, we can study the impact of the normalized separation on the previous distribution (see Figure 6, right panel). The normalized separation N_{sep} is the angular separation between the Gaia EDR3 and ICRF3 positions, normalized by its formal uncertainty [5]. The higher the normalized separation, the more precise the Gaia-ICRF3 offset vector angle. For the sources with $N_{sep} < 2\sigma$, no particular alignment is found. The peak around 0° becomes slightly visible for $N_{sep} \sim 2\sigma$ and that around 180° for $N_{sep} \sim 3\sigma$. At the highest values of the normalized separation ($N_{sep} > 6\sigma$), all sources but a small portion (4%) show alignment between the jet directions and Gaia-ICRF3 offset vectors. By examining individual maps for this fraction of sources, we note that 75% of them show no jet or have a two-sided jet, which can thus lead to an incorrect determination of the jet direction. The remaining 25% are not yet understood and will have to be investigated in more detail.

5 Conclusion

We developed a fully automatic method to determine source jet directions directly from VLBI images. This method was successfully applied to all available BVID images at S, X, K, and Q band, resulting in the production of 9,215 jet directions for 1,221 sources. From these directions, we further computed the mean jet direction over all epochs for each source. Comparing the mean jet directions at X-band with the Gaia EDR3 (optical)-ICRF3 S/X-band (radio) offset vector directions confirms that the two directions are aligned within 30° in roughly half of the sources.

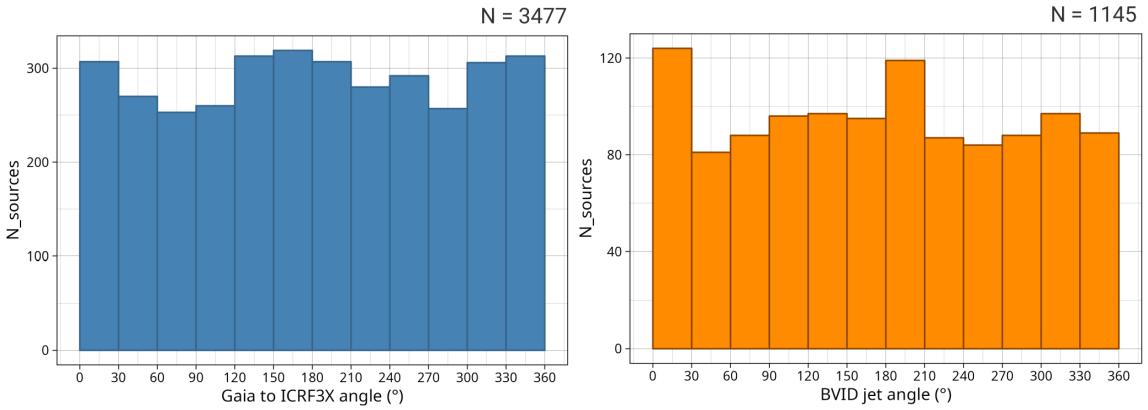

Fig. 5 Distributions of the Gaia EDR3 to ICRF3 S/X-band offset vector angles (left) and BVID jet directions at X-band (right).

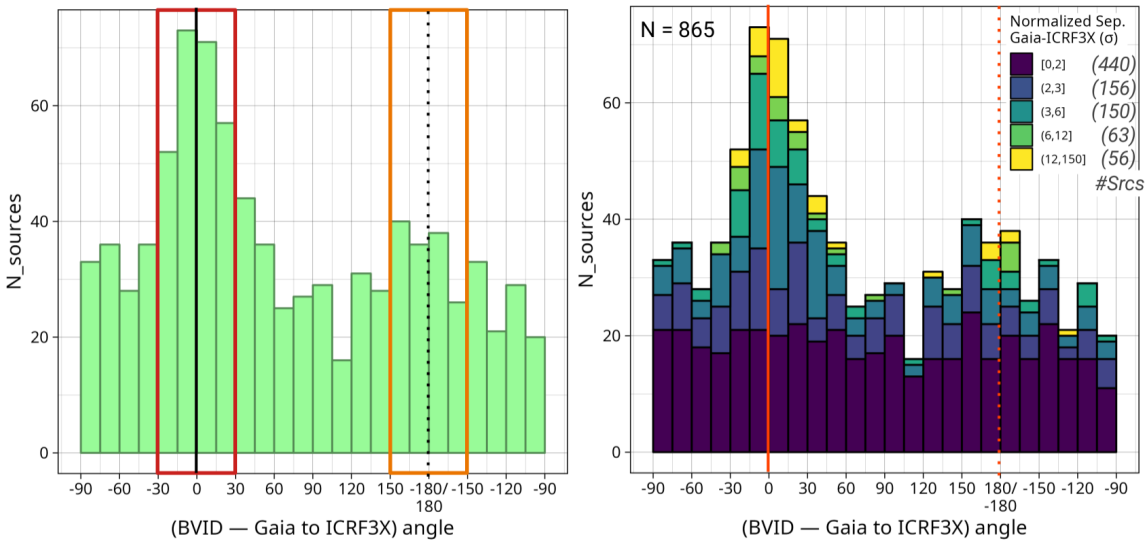

Fig. 6 (Left) Distribution of the differences (BVID − Gaia EDR3 to ICRF3 S/X-band offset vector directions). The optical-radio offset vectors are aligned within a range of ±30° (indicated by the colored rectangles) with the jet directions in 393 sources. (Right) The same distribution color-coded according to the normalized separation. The alignment is preferentially visible for the highest normalized separations.

Future prospects include studying the variability of the jet directions with time, comparing the jet directions between frequency bands, and comparing the Gaia EDR3-ICRF3 offset vector angles to the jet directions at K band.

References

1. A. Collioud, P. Charlot, Proceedings of the 19th EVGA Working Meeting, 24-25 March 2009, Bordeaux, France, Eds G. Bourda, P. Charlot and A. Collioud, pp. 19–22, 2009.
2. A. Collioud, P. Charlot, Proceedings of the 24th EVGA Working Meeting, 17-19 March 2019, Las Palmas de Gran Canaria, Spain, Eds R. Haas, S. Garcia-Espada, and J.A. López Fernández, pp. 219–223, 2019.
3. S.A. Klioner et al., A&A, forthcoming article, DOI: 10.1051/0004-6361/202243483, 2022.
4. S. Lambert et al., A&A, 651, A64, DOI: 10.1051/0004-6361/202140652, 2021.
5. P. Charlot et al., A&A, 644, A159, DOI: 10.1051/0004-6361/202038368, 2020.
6. Y. Kovalev, L. Petrov, A. Plavin, A&A, 598, L1, DOI: 10.1051/0004-6361/201630031, 2017.
7. A. Plavin, Y. Kovalev, L. Petrov, ApJ, 871, 143, DOI: 10.3847/1538-4357/aaf650, 2019.
8. L. Petrov, Y. Kovalev, A. Plavin, MNRAS, 482, 3023, DOI: 10.1093/mnras/sty2807, 2019.
9. Xu et al., A&A, 647, A189, DOI: 10.1051/0004-6361/202040168, 2021.